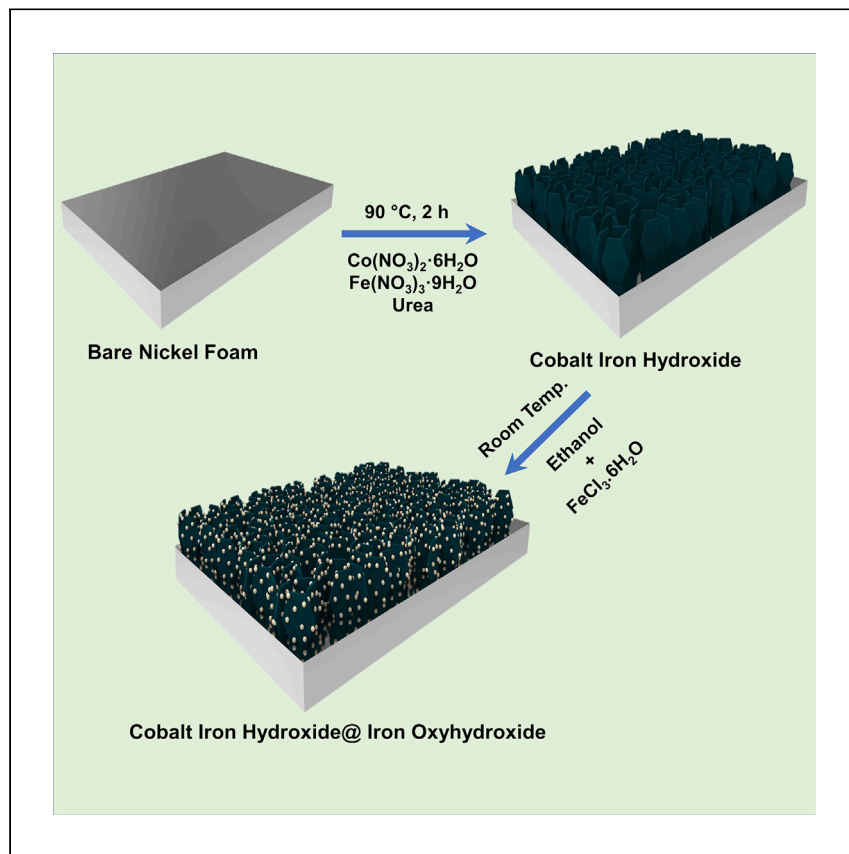


**Article**

# Low-overpotential overall water splitting by a cooperative interface of cobalt-iron hydroxide and iron oxyhydroxide



An interface engineering electrode consisting of CoFe-OH and FeOOH on a nickel foam substrate is developed as an efficient bifunctional electrocatalyst for overall water splitting by Babar et al. CoFe-OH@FeOOH shows notable performance for overall water splitting with a low potential of 1.56 V at  $10 \text{ mA cm}^{-2}$ .

Pravin Babar, Komal Patil,  
Javeed Mahmood, Seok-jin Kim,  
Jin Hyeok Kim, Cafer T. Yavuz

jinhyeok@chonnam.ac.kr (J.H.K.)  
cafer.yavuz@kaust.edu.sa (C.T.Y.)

## Highlights

Efficient CoFe-OH@FeOOH  
electrocatalyst for overall water  
splitting

Interface coupling may tailor  
electronic structure

CoFe-OH@FeOOH delivers a cell  
voltage of 1.56 V for overall water  
splitting

Babar et al., Cell Reports Physical Science 3,  
100762  
February 16, 2022 © 2022 The Authors.  
<https://doi.org/10.1016/j.xcrp.2022.100762>



Article

# Low-overpotential overall water splitting by a cooperative interface of cobalt-iron hydroxide and iron oxyhydroxide

Pravin Babar,<sup>1,2</sup> Komal Patil,<sup>3</sup> Javeed Mahmood,<sup>2</sup> Seok-jin Kim,<sup>1,2</sup> Jin Hyeok Kim,<sup>3,\*</sup> and Cafer T. Yavuz<sup>1,2,4,\*</sup>

## SUMMARY

Interface engineering is a powerful strategy for modulating electronic structure and enhancing intrinsic activity of electrocatalysts for water splitting. Here, we grow two-dimensional cobalt-iron hydroxide (CoFe-OH) nanosheets on nickel foam substrates and deposit FeOOH nanoparticles in a rapid and scalable wet chemical approach. The CoFe-OH@FeOOH nanocomposite features abundant active sites and high surface area, allowing fast kinetics for electrochemical water splitting. The electrode has a low overpotential value of 200 mV at 50 mA cm<sup>-2</sup> for oxygen evolution. When used as both anode and cathode for overall water splitting, CoFe-OH@FeOOH provides a low cell voltage of 1.56 V to deliver 10 mA cm<sup>-2</sup> current density. The synergistic activity is presumed to be from the seamless interface of CoFe-OH and FeOOH, improving conductivity and mass transfer. We envision that this simple approach may offer a new direction for designing efficient electrodes for energy conversion applications.

## INTRODUCTION

Hydrogen is a key ingredient for current industrial processes such as synthesis of ammonia and refining of petrol, and a promising fuel for a renewable and sustainable future.<sup>1–3</sup> Considering its promise in carbon-free and renewable characteristics, hydrogen is an ideal next-generation energy carrier, if it is produced by electrochemical water splitting.<sup>4–7</sup> Water electrolysis, therefore, has attracted widespread attention despite being energy intensive.<sup>8–12</sup> To lower the electrolytic cost, the potential required for the two half-cell reactions of water electrolysis, anodic oxygen evolution reaction (OER) and cathodic hydrogen evolution reaction (HER), ought to be lowered.<sup>13–15</sup> The OER and HER processes involve complex multielectron transfer mechanisms, resulting in high anodic and cathodic overpotentials.<sup>16–18</sup> Precious-metal-based electrodes have so far been benchmarks for HER and OER.<sup>19–22</sup> However, the high cost, low availability, and inferior durability prohibit large-scale applications.<sup>23–25</sup> Thus, developing an inexpensive, earth-abundant electrocatalyst with high efficiency and stability in overall water splitting is desirable.

Currently, water-splitting research is mainly focused on enhancing electrochemical performance with low overpotential while reducing the fabrication costs using earth-abundant electrode materials. The transition-metal-based electrodes are preferable alternatives to noble metals, and considerable efforts have been made to explore cobalt-iron (CoFe)-based materials as bifunctional electrocatalysts for water electrolysis. At present, the CoFe-based electrode materials mainly include oxide,

<sup>1</sup>KAUST Catalysis Center, Physical Sciences and Engineering (PSE), King Abdullah University of Science and Technology (KAUST), Thuwal 23955, Saudi Arabia

<sup>2</sup>Advanced Membranes and Porous Materials Center (AMPMC), Physical Sciences and Engineering (PSE), King Abdullah University of Science and Technology (KAUST), Thuwal 23955, Saudi Arabia

<sup>3</sup>Optoelectronic Convergence Research Center, Department of Materials Science and Engineering, Chonnam National University, Gwangju 500-757, South Korea

<sup>4</sup>Lead contact

\*Correspondence:  
[jinhyeok@chonnam.ac.kr](mailto:jinhyeok@chonnam.ac.kr) (J.H.K.),  
[cafer.yavuz@kaust.edu.sa](mailto:cafer.yavuz@kaust.edu.sa) (C.T.Y.)

<https://doi.org/10.1016/j.xcpr.2022.100762>



hydroxide, nitride, and phosphide.<sup>26–33</sup> Among these candidates, 2D CoFe hydroxide (CoFe-OH) has attracted widespread attention. Such growing interest is associated with its abundance of active sites, rich redox chemistry, and synergy between Co and Fe metal ions.<sup>34</sup> The synergic effect in bimetallic hydroxide (CoFe-OH) could also provide a better coordination environment and effective interaction with Co and Fe ions and improve charge transferability to enhance catalytic performance.<sup>31,32</sup> However, the catalytic activity and stability of CoFe-OH remain far from ideal compared with noble-metal-based catalysts, demanding further performance improvement. Recent strategies include improving the catalytic activity of CoFe-OH by optimizing chemical composition, enhancing conductivity by including carbon-based supporting materials, or exfoliating the nanosheets.<sup>35–38</sup> Despite these advances, CoFe-OH electrocatalysts still require a significant overpotential for overall water splitting. To achieve a low overpotential for overall water splitting, modification of the surface properties of the electrode materials is essential.<sup>39</sup> The efficient catalysts should have a surface with optimal adsorption energetics, which is neither too weak nor too strong.<sup>40,41</sup> In this regard, interface engineering provides an excellent tool to regulate surface properties.<sup>42,43</sup> Another effective way to improve the electrochemical performance of the catalyst would be to grow the electrode materials on a 3D conductive nickel foam (NF) (2D nanosheets), which, in turn, could provide a high density of active sites and robust mechanical structure.<sup>44,45</sup>

In combination with all these key discoveries, we herein prepared a composite electrode by anchoring FeOOH nanoparticles onto CoFe-OH nanosheets to construct a CoFe-OH@FeOOH interface structure for overall water splitting. In this simple and scalable fabrication of the heterogeneous interface electrocatalyst, the electronic environment is optimally modulated for enhanced electrochemical activity. The new CoFe-OH@FeOOH electrocatalyst revealed remarkable electrocatalytic activity toward OER with a low overpotential of 200 mV to deliver 50 mA cm<sup>-2</sup> current density with high stability for at least 50 h at a constant current density of 50 mA cm<sup>-2</sup>. Furthermore, the cell voltage for overall water splitting of CoFe-OH@FeOOH at 10 mA cm<sup>-2</sup> current density was 1.56 V, much lower than that for all other CoFe-based catalysts.

## RESULTS AND DISCUSSION

### Synthesis and characterization

The synthesis of CoFe-OH@FeOOH involves two steps as illustrated in Figure 1. In the first step, CoFe-OH nanosheet arrays are uniformly deposited on the NF substrate by a simple chemical bath deposition (CBD) at 90°C for 2 h. FeOOH is deposited on the CoFe-OH nanosheets through a simple wet chemical method in the second step, as described in the [experimental procedures](#). The CoFe-OH films were initially characterized by X-ray diffraction (XRD) to confirm the formation of the structure. Figure 1A shows the powder XRD patterns of CoFe-OH@FeOOH and CoFe-OH. The peaks (2θ) at 44.5°, 52°, and 76.3° arise from metallic Ni of the NF substrate corresponding to (111), (200), and (220) lattice planes (JCPDS 04-850).<sup>46</sup> The diffraction peaks located at 11.3°, 23.2°, 34°, and 60.4° can be assigned to the (003), (006), (012), and (113) planes of CoFe-OH (JCPDS 50-0235).<sup>47</sup> After FeOOH deposition on CoFe-OH, the diffraction peaks of CoFe-OH@FeOOH are the same as those of CoFe-OH, suggesting that FeOOH deposition does not change the crystal structure of pre-deposited CoFe-OH. But the intensity of the CoFe-OH peaks was not as high, suggesting the less crystallized nanostructure of CoFe-OH@FeOOH, and the slight shift of the peaks was also noted to lower the 2θ values. To further examine the crystallinity of the FeOOH species alone, a control NF film with only FeOOH deposition

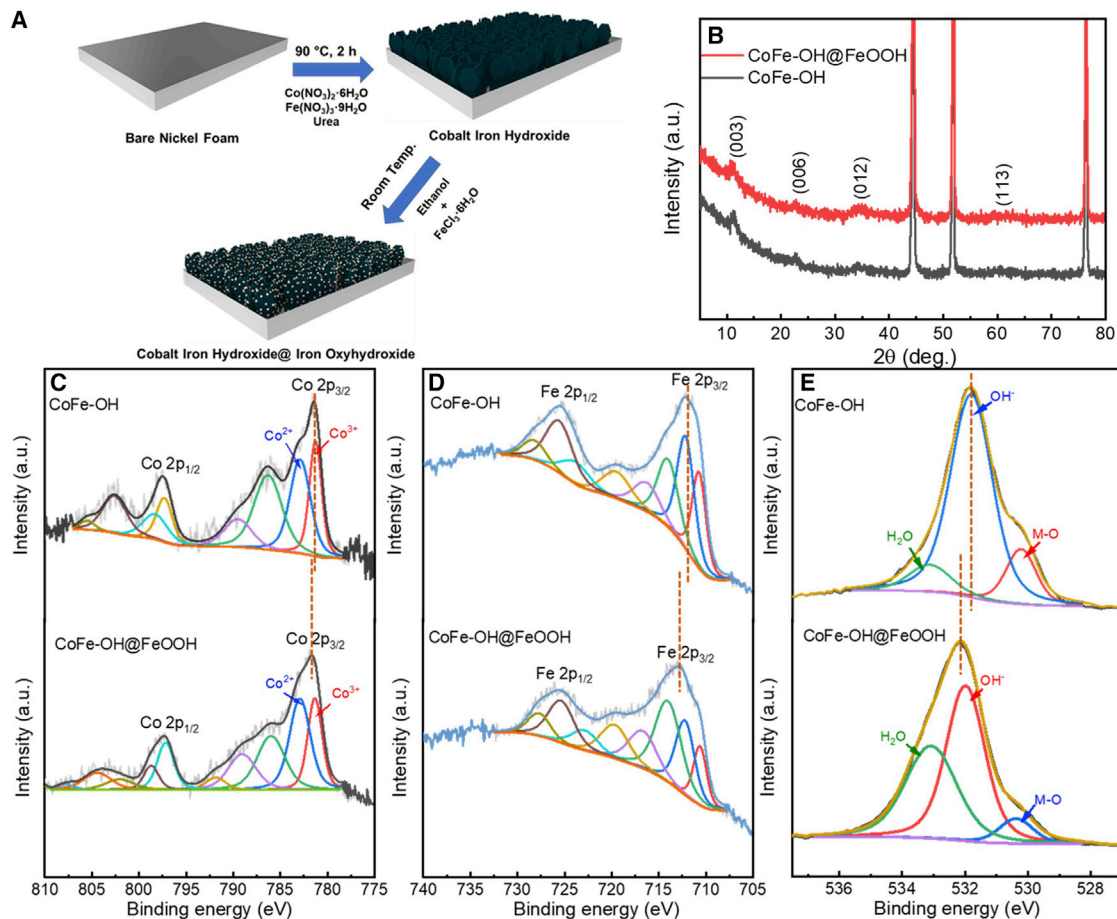


**Figure 1. Synthesis and characterization of CoFe-OH@FeOOH**

- (A) Schematic illustration of the fabrication process for CoFe-OH@FeOOH electrode.
- (B) XRD patterns of CoFe-OH and CoFe-OH@FeOOH.
- (C–E) High-resolution XPS spectra of (C) Co 2p, (D) Fe 2p, and (E) O 1s for CoFe-OH and CoFe-OH@FeOOH.

was examined with powder XRD. As shown in Figure S1, no new peaks specific to FeOOH were observed, demonstrating that no crystalline FeOOH nanoparticles could be detected in the electrocatalysts studied in this work.

The electronic interaction between CoFe-OH nanosheets and FeOOH nanoparticles was investigated using X-ray photoelectron spectroscopy (XPS). The high-resolution XPS spectra of CoFe-OH and CoFe-OH@FeOOH are shown in Figures 1C–1E. The binding energies of Co 2p<sub>3/2</sub> and Co 2p<sub>1/2</sub> in CoFe-OH are located at 781.4 and 797.5 eV, respectively, along with their satellite peaks. After CoFe-OH@FeOOH formation the binding energy of Co 2p<sub>3/2</sub> (781.7 eV) shows a positive shift in contrast to pure CoFe-OH (Figure 1C), suggesting a strong interaction between CoFe-OH and FeOOH. Also, the peak fitting reveals the co-existence of Co<sup>2+</sup> (784.3 eV) and Co<sup>3+</sup> (782.9 eV) in both films. Meanwhile, the CoFe-OH@FeOOH has higher Co<sup>2+</sup>/Co<sup>3+</sup> peak intensity compared with CoFe-OH, indicating that more Co<sup>2+</sup> is present in the CoFe-OH@FeOOH.<sup>48,49</sup> Similarly, the Fe 2p<sub>3/2</sub> of CoFe-OH@FeOOH (712.7 eV) shows a positive shift in binding energy compared with CoFe-OH (712.2 eV). The peak fitting of Fe 2p for as-prepared CoFe-OH indicates two distinct Fe species, at 712.2 (Fe 2p<sub>3/2</sub>) and 725.6 eV (Fe 2p<sub>1/2</sub>) (Figure 1D). However, the Fe 2p<sub>3/2</sub> peak

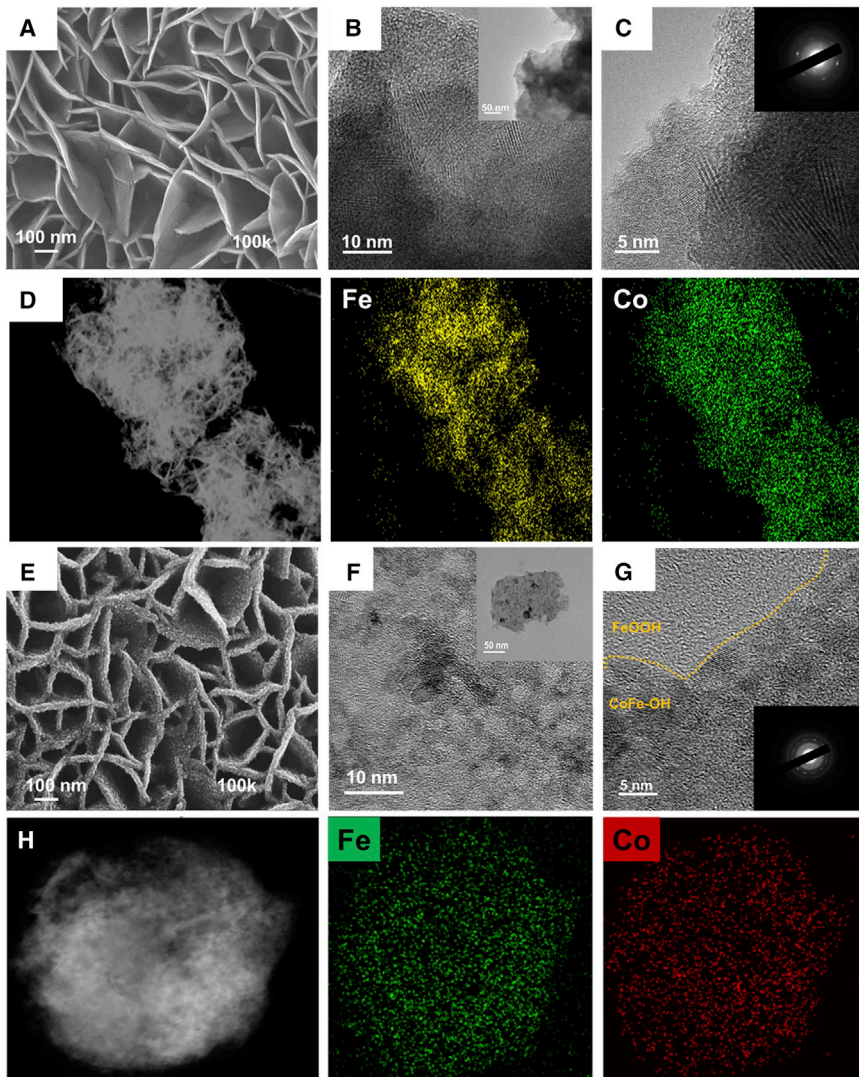
was at 712.8 eV for CoFe-OH@FeOOH. This positive shift in Fe 2p<sub>3/2</sub> indicates the increase in electron density around the Fe atoms in CoFe-OH@FeOOH as opposed to CoFe-OH due to elevated oxygen vacancy.<sup>50</sup> The high-resolution O 1s spectrum further confirms oxygen vacancies in CoFe-OH@FeOOH. The O 1s spectrum shows prominent characteristic peaks at 530.2, 531.8, and 533.2 eV corresponding to metal-oxygen (M-O), oxygen defects (OH<sup>-</sup>), and water molecules absorbed on the surface (H<sub>2</sub>O), respectively (Figure 1E).<sup>51</sup> The O 1s spectrum in CoFe-OH@FeOOH shows decreased peak intensity for OH<sup>-</sup> and increased intensity for absorbed water, which further reinforces the presence of oxygen vacancies.<sup>52,53</sup> The peak shifts in XPS spectra reveal the electronic structure modification of the electrocatalyst, which relies on strong electronic interplay between CoFe-OH and FeOOH. The strong electronic interaction indicates the synergistic effect between CoFe-OH and FeOOH, which is known to assist during interface events (e.g., water adsorption) to enhance OER and HER efficiency.<sup>54,55</sup>

Figure 2A shows the field emission SEM (FE-SEM) image of CoFe-OH, which indicates that nanosheets are grown vertically on the NF substrate, and the interconnected nanosheets have smooth surfaces. The transmission electron microscopy (TEM) image (Figure 2B) further demonstrates the distinct nanosheet morphology of CoFe-OH. The high-resolution TEM (HR-TEM) image as shown in Figure 2C of CoFe-OH indicates well-resolved lattice fringes with an interplanar spacing of 2.6 nm, corresponding to the (101) plane of CoFe-OH. The selected-area electron diffraction (SAED) pattern shows the crystalline nature of the CoFe-OH film (inset in Figure 2C). Figure 2D displays the energy-dispersive X-ray spectroscopy (EDX) mapping images of CoFe-OH demonstrating the presence of Co and Fe throughout the nanosheet. After FeOOH deposition on CoFe-OH, the FE-SEM image (Figure 2E) indicates that the surface of nanosheets becomes rough with nanoparticles anchored on, compared with the pristine surface of CoFe-OH. The TEM image of CoFe-OH@FeOOH further confirms that the nanoparticles are immobilized on the CoFe-OH surface (Figure 2F). The HR-TEM images reveal the lattice disturbance, suggesting the low crystallinity of CoFe-OH film (Figure 2G). The SAED pattern shows the weak diffraction ring, which further confirms the low crystallinity of CoFe-OH@FeOOH. EDX-mapping images of CoFe-OH@FeOOH (Figure 2H) reveal the uniform distribution of Co and Fe throughout the heterostructures, further indicating the successful preparation of CoFe-OH@FeOOH. From the analysis thus far, we conclude that the surface of nanosheets has been notably changed while preserving the main crystalline nature of CoFe-OH without forming any new, crystalline phases.

To gain an insight into the formation of CoFe-OH@FeOOH, we varied the FeOOH deposition time (Figures 3 and S2). When the reaction time is only 5 min, nanosheet surfaces are a little rough compared with the plain nanosheet morphology of CoFe-OH. Subsequently, when the synthesis time is 10 min, the nanosheets are observed to have nanoparticles anchored on the surface. With further increase in the reaction time, the nanoparticles are uniformly deposited on the surface of nanosheets (20–40 min). Furthermore, the powder XRD pattern (Figure S2) shows that the peak intensity of CoFe-OH decreases with increase in reaction time, and peak locations are slightly shifted to lower 2θ values. We can thus expect that CoFe-OH@FeOOH could improve the electrochemical performance of overall water splitting by boosting intrinsic activity.

### OER activity

To understand how interface engineering affects the OER performance of CoFe-OH@FeOOH, the electrochemical properties of the catalysts were investigated in a three-electrode system in a 1 M KOH electrolyte. For comparison, CoFe-OH,



**Figure 2. Electron microscopy characterization of the electrocatalysts**

(A–D) (A) FE-SEM, (B) TEM, (C) HR-TEM (inset, SAED), and (D) EDX mapping of CoFe-OH. (E–H) (E) FE-SEM, (F) TEM, (G) HR-TEM (inset, SAED), and (H) EDX mapping of CoFe-OH@FeOOH.

FeOOH, RuO<sub>2</sub>, and bare NF films were also tested under the same experimental conditions. The linear sweep voltammetry (LSV) curves with *iR* correction are displayed in Figure 4A. The LSV curve reveals that CoFe-OH@FeOOH delivers the highest current density and lowest overpotential among the controls, achieving current densities of 50 and 100 mA cm<sup>-2</sup> at low overpotentials of 200 and 230 mV, respectively. These values are much lower than those of CoFe-OH (230 and 255 mV), FeOOH (255 and 270 mV), and RuO<sub>2</sub> (250 and 275 mV) at the same current densities. The as-prepared CoFe-OH@FeOOH nanosheet arrays also exhibit better OER performance than that of other recently reported non-precious-metal electrocatalysts (Table S1).

Tafel slopes of all tested catalysts are shown in Figure 4B, indicating a significant improvement in the OER kinetics, consistent with the OER performance of the new catalysts. The Tafel slope of CoFe-OH@FeOOH was 48 mV dec<sup>-1</sup>, which is much smaller

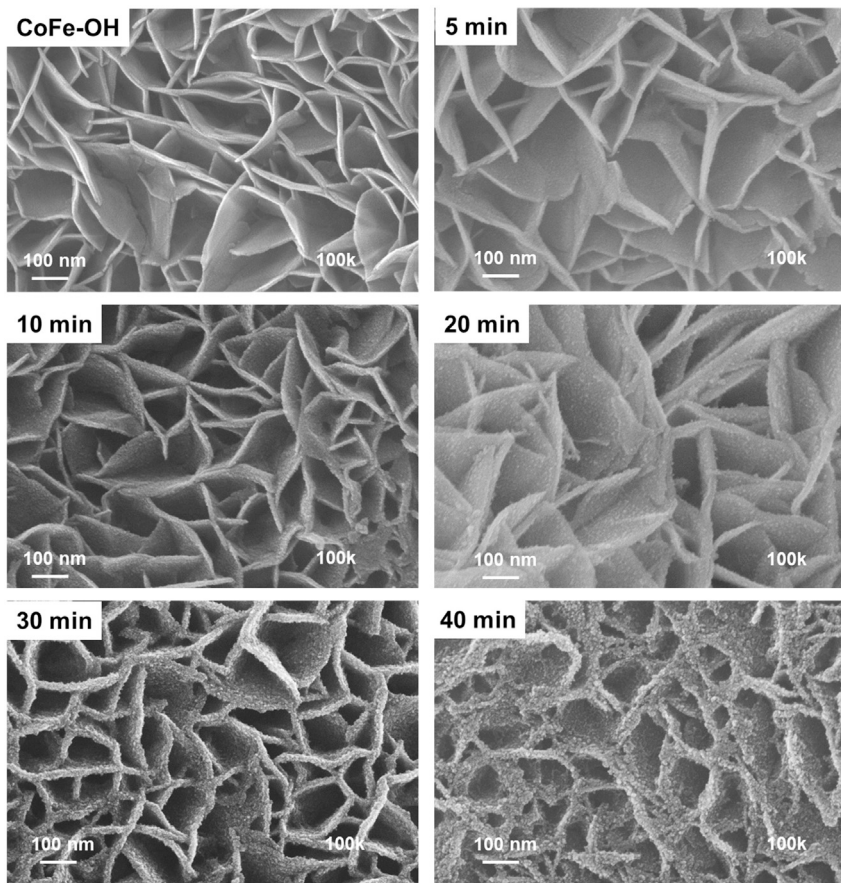


**Figure 3. FE-SEM images**

FE-SEM images of CoFe-OH@FeOOH after various FeOOH deposition times.

compared with CoFe-OH ( $73 \text{ mV dec}^{-1}$ ), FeOOH ( $86 \text{ mV dec}^{-1}$ ), RuO<sub>2</sub> ( $83 \text{ mV dec}^{-1}$ ), and bare NF ( $114 \text{ mV dec}^{-1}$ ), suggesting the kinetically favored nature of the CoFe-OH@FeOOH film.<sup>56</sup> These results indicate that the OER efficacy of CoFe-OH remarkably improved after the construction of the CoFe-OH@FeOOH interface.

The OER performances of CoFe-OH@FeOOH, CoFe-OH, FeOOH, RuO<sub>2</sub>, and bare NF are compared in Figure 4C. Although CoFe-OH, FeOOH, and RuO<sub>2</sub> show good OER performance, with 255, 270, and 275 mV to achieve  $100 \text{ mA cm}^{-2}$  current density, respectively, their combination, CoFe-OH@FeOOH, demonstrates even more enhanced OER activity, with a lower overpotential of 230 mV at the same current density. In addition, the OER activity of CoFe@FeOOH at a different reaction time with FeOOH was also studied (Figure S3). The CoFe@FeOOH at 30 min FeOOH deposition shows excellent catalytic activity, with low overpotential and Tafel slope compared with other electrocatalysts. In the multistep chronopotentiometry curve of CoFe-OH@FeOOH in 1 M KOH (Figure 4D), the current density increases from 80 to 170  $\text{mA cm}^{-2}$  with increments of  $10 \text{ mA cm}^{-2}$  per 500 s. The potential immediately levels off and remains constant for 500 s, indicating excellent mass transport, mechanical robustness, and good conductivity of the CoFe-OH@FeOOH electrode.<sup>57</sup> Taking it further, we studied the long-term durability of CoFe-OH@FeOOH for 50 h at a high current density of  $50 \text{ mA cm}^{-2}$ . Figure 4E shows the activity of the CoFe-OH@FeOOH catalyst remaining stable during a 50-h continuous OER electrolysis, while the LSV polarization curves

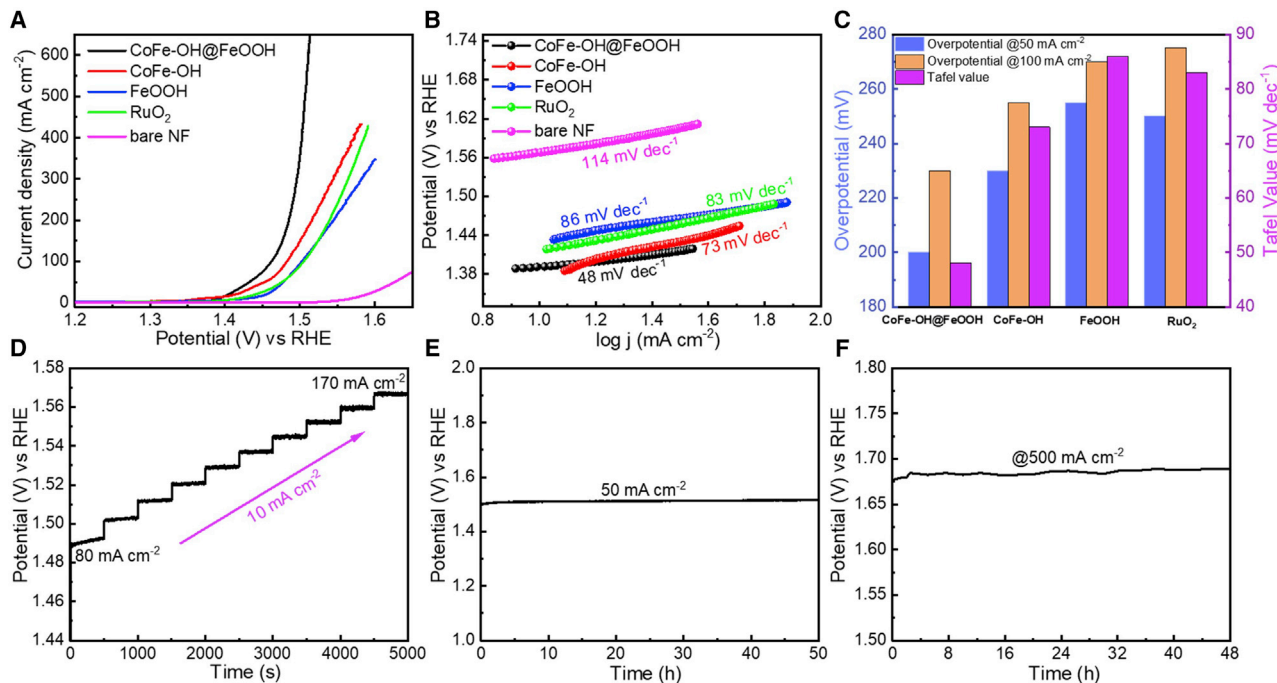


**Figure 4. Electrochemical OER performance**

- (A) *iR*-corrected polarization curves in 1.0 M KOH solution.
- (B) Tafel plots derived from the corresponding polarization curves.
- (C) Comparison of the overpotential and Tafel slopes.
- (D) Multicurrent process of CoFe-OH@FeOOH (without *iR* correction).
- (E) Chronopotentiometry stability test of CoFe-OH@FeOOH over 50 h at a constant current density of 50 mA cm<sup>-2</sup> (without *iR* correction).
- (F) Chronopotentiometry stability test of CoFe-OH@FeOOH over 48 h at a constant current density of 500 mA cm<sup>-2</sup> (without *iR* correction).

before and after the long-term stability test are almost overlapping each other (Figure S4). At a higher current density of 500 mA cm<sup>-2</sup>, the as-prepared CoFe-OH@FeOOH also shows excellent stability (Figure 4F).

### HER activity

The HER activity of the CoFe-OH@FeOOH catalyst was also conducted in the same electrolyte (1 M KOH), for consistency and the goal of providing overall water-splitting performance. As expected, bare NF has poor catalytic activity for HER (Figure 5A). The LSV polarization curve of CoFe-OH@FeOOH exhibits a low overpotential of 145 mV at 10 mA cm<sup>-2</sup> compared with CoFe-OH (185 mV), FeOOH (205 mV), and bare NF (247 mV) at the same current density. Noticeably, the cathodic current induced by CoFe-OH@FeOOH largely surpasses that of CoFe-OH and FeOOH.

The Tafel slope determines the inherent kinetics of the HER cathode. The CoFe-OH@FeOOH catalyst possesses a Tafel slope of 51 mV dec<sup>-1</sup>, even smaller than those of CoFe-OH (58 mV dec<sup>-1</sup>), FeOOH (65 mV dec<sup>-1</sup>), and bare NF (86 mV dec<sup>-1</sup>), implying more favorable kinetics of CoFe-OH@FeOOH during the HER process (Figure 5B). The electrocatalytic HER performance of CoFe-OH@FeOOH is better than or comparable to that of the recently reported HER catalysts (Table S2). Moreover, the multicurrent step curve of CoFe-OH@FeOOH at current densities from 80 to 170 mA cm<sup>-2</sup> was also checked with increasing 10 mA cm<sup>-2</sup> current density for 500 s (Figure 5D). The potential of CoFe-OH@FeOOH increases and stabilizes at all ranges of current densities. This fast response indicates the excellent

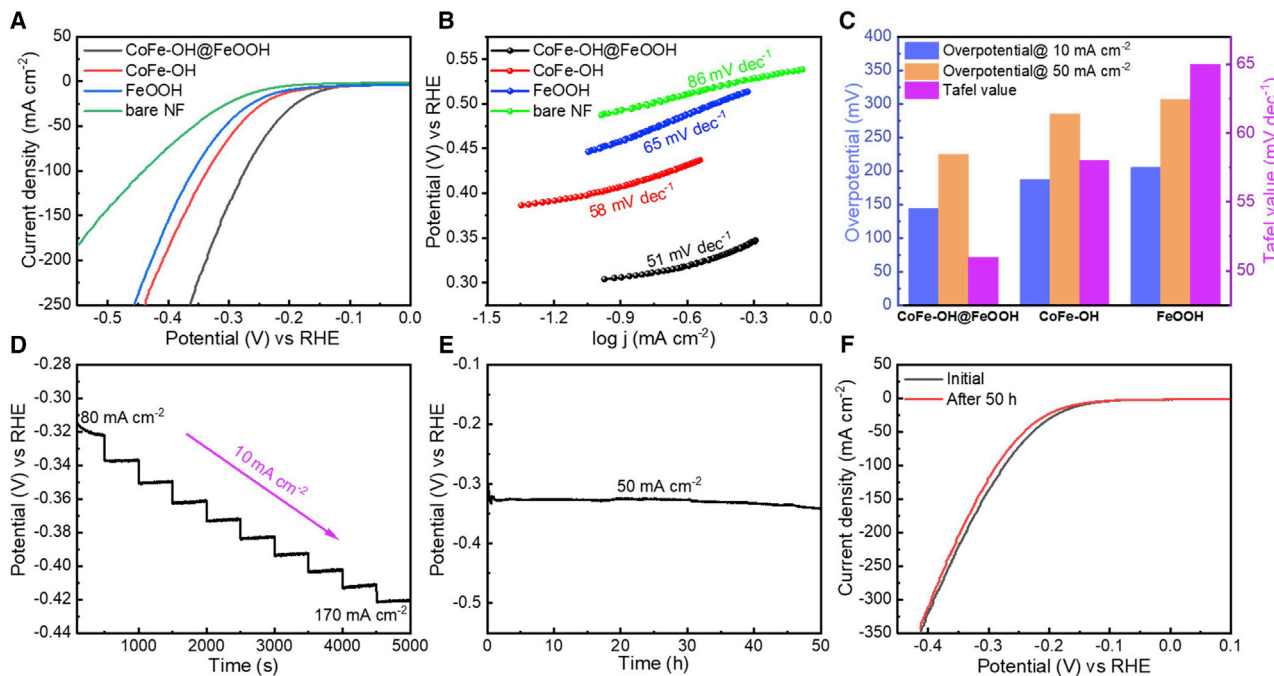


**Figure 5. Electrochemical HER performance**

- (A)  $iR$ -corrected polarization curves.
- (B) Tafel plots derived from the corresponding polarization curves.
- (C) Comparison of the overpotential and Tafel slopes.
- (D) Multicurrent process of CoFe-OH@FeOOH (without  $iR$  correction).
- (E) Chronopotentiometry stability test of CoFe-OH@FeOOH over 50 h at a constant current density of  $50 \text{ mA cm}^{-2}$  (without  $iR$  correction).
- (F) Polarization curves of CoFe-OH@FeOOH before and after 50-h stability test.

mechanical stability and mass transfer of the electrocatalyst.<sup>58</sup> Another critical parameter, the long-term stability of the CoFe-OH@FeOOH catalyst, was investigated by a continuous potential cycling at a constant current density of  $50 \text{ mA cm}^{-2}$  (Figure 5E). It was observed that CoFe-OH@FeOOH maintained almost the same potential even after 50 h. During the 50 h of testing, CoFe-OH@FeOOH exhibited a slight potential fluctuation at  $50 \text{ mA cm}^{-2}$  current density (Figure 5F). Furthermore, the CoFe-OH@FeOOH catalyst was analyzed by FE-SEM and XPS after a long-term durability test. The FE-SEM images of CoFe-OH@FeOOH under different magnifications clearly suggest that the morphology of the nanosheet structure was preserved (Figure S5). After the long-term durability test, the XPS spectra of Co, Fe, and O indicate similar binding energies without any peak shift (Figure S6), which signifies that the CoFe-OH@FeOOH catalyst has excellent electrochemical stability.

The combination of robust intrinsic activity and the abundance of exposed active sites of catalyst enhances the efficiency of a catalyst.<sup>59</sup> In electrocatalysis, inherent activity and the amount of exposed active sites can be calculated using turnover frequency (TOF) and electrochemical surface area (ECSA).<sup>60</sup> TOF value is estimated by taking the exact number of electrochemical accessible sites using a cyclic voltammetry (CV) curve (Figures 6A and S7). The TOF values of all the studied catalysts were calculated at various potentials (Figure 6B). The TOF value of CoFe-OH@FeOOH was  $144 \text{ s}^{-1}$  at the potential of 1.50 V versus reversible hydrogen electrode (RHE), which is higher than both CoFe-OH ( $104 \text{ s}^{-1}$ ) and FeOOH ( $92 \text{ s}^{-1}$ ) at the same potential (inset in Figure 6B). The ECSA is directly proportional to the double-layer capacitance ( $C_{dl}$ ) of the catalyst, which is

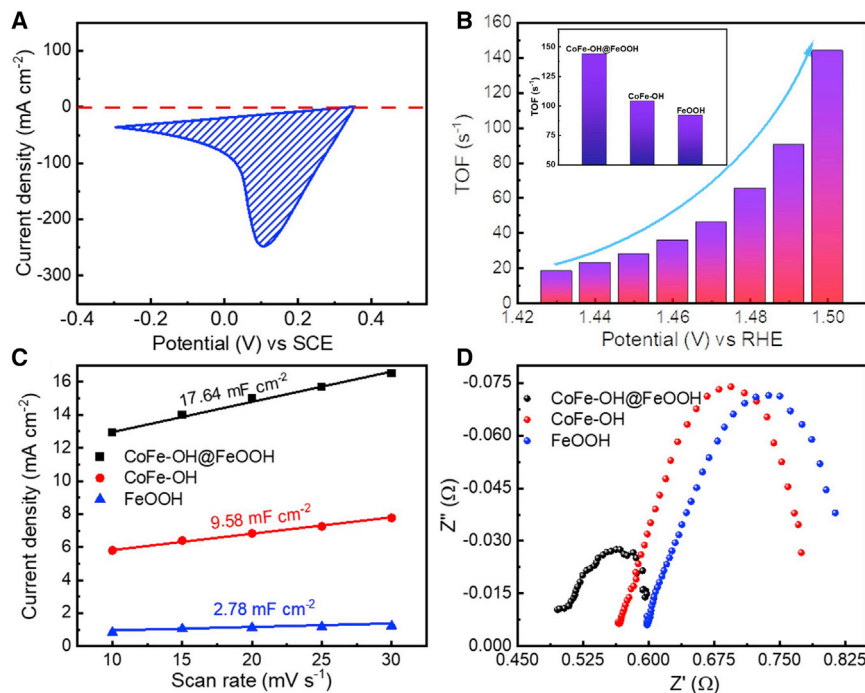


**Figure 6. Calculation of active sites and TOF**

- (A) Backward CV of CoFe-OH@FeOOH for charge integration and calculation of electrochemically accessible sites.
- (B) TOF values at various potentials for CoFe-OH@FeOOH. Inset: TOF values for CoFe-OH@FeOOH, CoFe-OH, and FeOOH at 1.5 V versus RHE.
- (C) Linear fit of the capacitive current versus scan rates for CoFe-OH@FeOOH, CoFe-OH, and FeOOH.
- (D) Nyquist plot of NiFeCo layered double hydroxide (LDH)/NF and NiFe LDH/NF.

calculated from CVs at different scan rates (Figure S8). As shown in Figure 6C, the  $C_{dl}$  value of CoFe-OH@FeOOH was  $17.64 \text{ mF cm}^{-2}$ , which is more than those of CoFe-OH ( $9.58 \text{ mF cm}^{-2}$ ) and FeOOH ( $2.78 \text{ mF cm}^{-2}$ ), owing to the exposure of more active sites from the vertically aligned structures. The TOF and ECSA results imply that interface-engineered CoFe-OH@FeOOH significantly increases intrinsic activity and the number of active sites. Electrochemical impedance spectroscopy (EIS) is used to evaluate the charge transfer across the electrode-electrolyte interface and other physicochemical processes. The Nyquist plot shows that the CoFe-OH@FeOOH electrode possesses a small  $R_{ct}$  ( $0.59 \Omega$ ) value compared with CoFe-OH ( $0.77 \Omega$ ) and FeOOH ( $0.81 \Omega$ ). This implies lower charge transfer resistance and faster kinetics, both of which make great contributions to enhancing the electrochemical performance (Figure 6D). The increase in ECSA and decrease in resistance of CoFe-OH@FeOOH compared with CoFe-OH and FeOOH are consistent with OER. In addition, the HER performance that indicates interface engineering facilitates highly active site exposure with fast electron transfer.

### Overall water splitting

The electrochemical measurements reveal that interface coupling of FeOOH and CoFe-OH significantly enhances the electrochemical activity for OER and HER. Thus, we assembled a full water-splitting cell using CoFe-OH@FeOOH as both an anode and a cathode. The CoFe-OH@FeOOH requires low cell voltages of only 1.56 and 1.72 V to reach current densities of 10 and  $50 \text{ mA cm}^{-2}$ , respectively, which

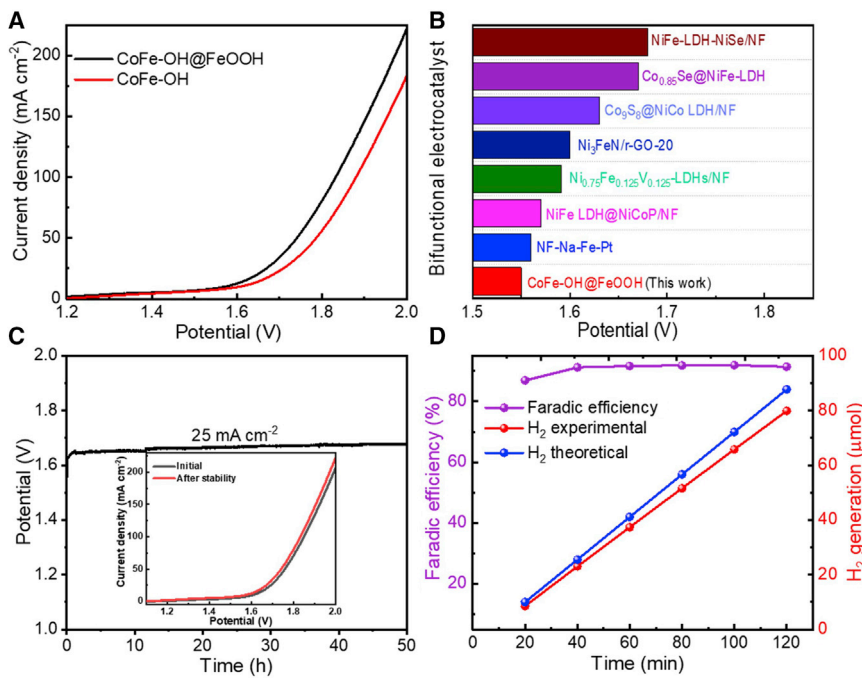


**Figure 7. Full electrochemical cell study for overall water splitting**

- (A) Polarization curves without *iR* compensation of CoFe-OH@FeOOH and CoFe-OH for overall water splitting in 1.0 M KOH electrolyte.
- (B) Comparison of this work and the recently reported bifunctional electrocatalysts at the current density of 10 mA cm<sup>-2</sup> in a two-electrode water-splitting system.
- (C) Long-term stability test of CoFe-OH@FeOOH at 25 mA cm<sup>-2</sup> for 50 h. Inset: the polarization curves before and after the long-term stability test.
- (D) Amount of H<sub>2</sub> theoretically calculated and experimentally measured and faradic efficiency versus time for CoFe-OH@FeOOH during overall water splitting.

are noticeably lower than those of CoFe-OH (1.62 and 1.78 V) for the same current density (Figure 7A). The performance of CoFe-OH@FeOOH for overall water splitting also surpasses most of the recently reported water-splitting cells (Figure 7B and Table S3).<sup>61–67</sup> The full-cell electrocatalytic stability of CoFe-OH@FeOOH was also investigated at 25 mA cm<sup>-2</sup> for 50 h (Figure 7C), showing outstanding stability. The LSV polarization curves were almost identical after 50 h of long-term stability (inset in Figure 7C), which further confirms the remarkable stability of the CoFe-OH@FeOOH electrode (Figures S9 and S10). The amount of H<sub>2</sub> evolved during overall water splitting was determined quantitatively by gas chromatography at a cell voltage of 1.8 V for 2 h (Figure 7D). The faradic efficiency, calculated from transferred charges and experimental measurements, reached 92%.

Figure 8 reveals the comparative activities of CoFe-OH and CoFe-OH@FeOOH for a comprehensive performance evaluation. The higher enclosed area means that the catalyst system has broad catalytic activity. The catalytic activity of CoFe-OH@FeOOH is substantially better than that of CoFe-OH. This remarkable catalytic performance of CoFe-OH@FeOOH could be ascribed to the following considerations: (1) the strong interaction between CoFe-OH and FeOOH could modulate the electronic structure and manipulate the catalytic behavior of Co<sup>2+</sup> to improve electrochemical performance. (2) CoFe-OH@FeOOH nanosheet-nanoparticle assembly leads to wider active-site exposure and enhances mass transfer. (3) The conductivity and intrinsic activity are enhanced after depositing FeOOH on CoFe-OH, thereby boosting electrochemical

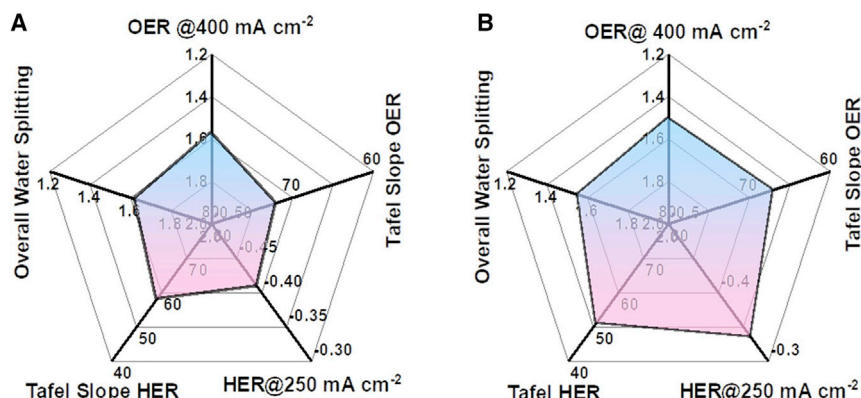


**Figure 8. Summary of the electrocatalytic performance**

- (A) CoFe-OH.
- (B) CoFe-OH@FeOOH.

performance. (4) CoFe-OH@FeOOH has a crystalline-amorphous interface and could modulate the CoFe-OH electronic structure, which could help optimize the adsorption energy to improve intrinsic electrocatalytic activity. (5) The direct growth of CoFe-OH@-FeOOH without any binders offers efficient binding between the electrode material and the NF substrate, providing good mechanical stability. Our investigations continue, to understand these mechanisms and beyond, for the ultimate goal of developing a sustainable electrochemical cell for overall water splitting.

In conclusion, we have designed a simple method to enhance the electrochemical performance of CoFe-OH nanosheets by decorating them with FeOOH nanoparticles. The positive effects of heterointerface and synergy generated between CoFe-OH and FeOOH allowed the CoFe-OH@FeOOH electrode to exhibit excellent electrocatalytic performance for overall water splitting. Significantly, the CoFe-OH@FeOOH electrode required an overpotential of only 200 mV to reach 50 mA cm<sup>-2</sup> current density for OER. Using the bifunctional CoFe-OH@FeOOH, the two-electrode full electrochemical cell required only 1.56 V to deliver 10 mA cm<sup>-2</sup> current density. Furthermore, after 50 h of continuous electrocatalytic stability tests, the catalytic performance of CoFe-OH@FeOOH remained almost the same, suggesting the excellent stability of the catalyst. This interface engineering approach could be extended to prepare low-cost and highly efficient electrodes for electrochemical energy conversion and storage application.

## EXPERIMENTAL PROCEDURES

### Resource availability

#### Lead contact

Further information and requests for resources and reagents should be directed to, and will be fulfilled by, the lead contact, Cafer T. Yavuz ([cafer.yavuz@kaust.edu.sa](mailto:cafer.yavuz@kaust.edu.sa)).

#### Materials availability

This study did not generate new unique reagents.

#### Data and code availability

The authors declare that data supporting the findings of this study are available within the article and the [supplemental information](#). All other data are available from the lead contact upon reasonable request.

## Materials

Cobalt nitrate hexahydrate (98%), iron nitrate nonahydrate (98%), urea (99%), hydrochloric acid (37%), and potassium hydroxide (KOH, ≥85%) were purchased from Sigma-Aldrich, USA. Solvents were used as received. Deionized water (DI) was collected from Milli-Q (18.2 MQ·cm at 25°C). NF substrates were acquired from Alantum (thickness, 1.6 mm; surface density, 420 g cm<sup>-2</sup>).

## Synthesis and characterization

Full experimental procedures are provided in the [supplemental experimental procedures](#).

## SUPPLEMENTAL INFORMATION

Supplemental information can be found online at <https://doi.org/10.1016/j.xcrp.2022.100762>.

## ACKNOWLEDGMENTS

This research was supported by the King Abdullah University of Science and Technology, Kingdom of Saudi Arabia, and by a Human Resources Development Program (20194030202470) of the Korea Institute of Energy Technology, Evaluation, and Planning (KETEP) grant funded by the Korean Government Ministry of Trade, Industry, and Energy, Republic of Korea.

## AUTHOR CONTRIBUTIONS

P.B., J.H.K., and C.T.Y. conceived and designed the idea. P.B. carried out the experiments and wrote the manuscript. K.P. provided assistance with the XRD and XPS characterizations. S.K. and J.M. participated in data analyses and discussions. All authors reviewed and contributed to this paper.

## DECLARATION OF INTERESTS

C.T.Y. is an advisory board member at *Cell Reports Physical Science*. The authors declare no other competing interests.

Received: October 22, 2021

Revised: December 15, 2021

Accepted: January 20, 2022

Published: February 16, 2022

## REFERENCES

- Gray, H.B. (2009). Powering the planet with solar fuel. *Nat. Chem.* 1, 7.
- Yuan, Z., Bak, S.M., Li, P., Jia, Y., Zheng, L., Zhou, Y., Bai, L., Hu, E., Yang, X.Q., Cai, Z., et al. (2019). Activating layered double hydroxide with multivacancies by memory effect for energy-efficient hydrogen production at neutral pH. *ACS Energy Lett.* 4, 1412–1418.
- Zhuang, L., Xu, F., Wang, K., Li, J., Liang, C., Zhou, W., Xu, Z., Shao, Z., and Zhu, Z. (2021). Porous structure engineering of iridium oxide nanoclusters on atomic scale for efficient pH-universal overall water splitting. *Small* 17, 2100121.
- Wu, A., Xie, Y., Ma, H., Tian, C., Gu, Y., Yan, H., Zhang, X., Yang, G., and Fu, H. (2018). Integrating the active OER and HER components as the heterostructures for the efficient overall water splitting. *Nano Energy* 44, 353–363.
- Ananthraj, S., Sugime, H., and Noda, S. (2021). Surface amorphized nickel hydroxy sulphide for efficient hydrogen evolution reaction in alkaline medium. *Chem. Eng. J.* 408, 127275.
- Huang, Y., Wei, G., He, J., An, C., Hu, M., Shu, M., Zhu, J., Yao, S., Xi, W., Si, R., et al. (2020). Interfacial electronic interaction of atomically dispersed IrCl<sub>x</sub> on ultrathin Co(OH)<sub>2</sub>/CNTs for efficient electrocatalytic water oxidation. *Appl. Catal. B Environ.* 279, 119398.
- Feng, J.-X., Xu, H., Dong, Y.-T., Ye, S.-H., Tong, Y.-X., and Li, G.-R. (2016). FeOOH/Co/FeOOH hybrid nanotube Arrays as high-performance electrocatalysts for the oxygen evolution reaction. *Angew. Chem. Int. Ed. Engl.* 128, 3758–3762.
- Li, G., Blake, G.R., and Palstra, T.T.M. (2017). Vacancies in functional materials for clean energy storage and harvesting: the perfect imperfection. *Chem. Soc. Rev.* 46, 1693–1706.
- Yu, F., Zhou, H., Huang, Y., Sun, J., Qin, F., Bao, J., Goddard, W.A., Chen, S., and Ren, Z. (2018). High-performance bifunctional porous non-noble metal phosphide catalyst for overall water splitting. *Nat. Commun.* 9, 1–9.
- Chen, P., Zhou, T., Zhang, M., Tong, Y., Zhong, C., Zhang, N., Zhang, L., Wu, C., and Xie, Y. (2017). 3D nitrogen-anion-decorated nickel sulfides for highly efficient overall water splitting. *Adv. Mater.* 29, 1701584.

11. Faber, M.S., and Jin, S. (2014). Earth-abundant inorganic electrocatalysts and their nanostructures for energy conversion applications. *Energy Environ. Sci.* 7, 3519–3542.
12. McCrory, C.C.L., Jung, S., Peters, J.C., and Jaramillo, T.F. (2013). Benchmarking heterogeneous electrocatalysts for the oxygen evolution reaction. *J. Am. Chem. Soc.* 135, 16977–16987.
13. Jiao, Y., Zheng, Y., Jaroniec, M., and Qiao, S.Z. (2015). Design of electrocatalysts for oxygen- and hydrogen-involving energy conversion reactions. *Chem. Soc. Rev.* 44, 2060–2086.
14. Sultan, S., Tiwari, J.N., Singh, A.N., Zhumagali, S., Ha, M., Myung, C.W., Thangavel, P., and Kim, K.S. (2019). Single atoms and clusters based nanomaterials for hydrogen evolution, oxygen evolution reactions, and full water splitting. *Adv. Energy Mater.* 9, 1900624.
15. Li, C.F., Zhao, J.W., Xie, L.J., Wu, J.Q., Ren, Q., Wang, Y., and Li, G.R. (2021). Surface-adsorbed carboxylate ligands on layered double hydroxides/metal-organic frameworks promote the electrocatalytic oxygen evolution reaction. *Angew. Chem. Int. Ed. Engl.* 60, 18129–18137.
16. Walter, M.G., Warren, E.L., McKone, J.R., Boettcher, S.W., Mi, Q., Santori, E.A., and Lewis, N.S. (2010). Solar water splitting cells. *Chem. Rev.* 110, 6446–6473.
17. Han, N., Liu, P., Jiang, J., Ai, L., Shao, Z., and Liu, S. (2018). Recent advances in nanostructured metal nitrides for water splitting. *J. Mater. Chem. A* 6, 19912–19933.
18. Nur Indah Sari, F., Abdillah, S., and Ting, J.M. (2021). FeOOH-containing hydrated layered iron vanadate electrocatalyst for superior oxygen evolution reaction and efficient water splitting. *Chem. Eng. J.* 416, 129165.
19. Reier, T., Oezaslan, M., and Strasser, P. (2012). Electrocatalytic oxygen evolution reaction (OER) on Ru, Ir, and Pt catalysts: a comparative study of nanoparticles and bulk materials. *ACS Catal.* 2, 1765–1772.
20. Lee, Y., Suntivich, J., May, K.J., Perry, E.E., and Shao-Horn, Y. (2012). Synthesis and activities of rutile  $\text{IrO}_2$  and  $\text{RuO}_2$  nanoparticles for oxygen evolution in acid and alkaline solutions. *J. Phys. Chem. Lett.* 3, 399–404.
21. Babar, P., Patil, K., Lee, D.M., Karade, V., Gour, K., Pawar, S., and Kim, J.H. (2021). Cost-effective and efficient water and urea oxidation catalysis using nickel-iron oxyhydroxide nanosheets synthesized by an ultrafast method. *J. Colloid Interface Sci.* 584, 760–769.
22. Gorlin, Y., and Jaramillo, T.F. (2010). A bifunctional nonprecious metal catalyst for oxygen reduction and water oxidation. *J. Am. Chem. Soc.* 132, 13612–13614.
23. Pawar, S.M., Pawar, B.S., Hou, B., Kim, J., Aqueel Ahmed, A.T., Chavan, H.S., Jo, Y., Cho, S., Inamdar, A.I., Gunjakar, J.L., et al. (2017). Self-assembled two-dimensional copper oxide nanosheet bundles as an efficient oxygen evolution reaction (OER) electrocatalyst for water splitting applications. *J. Mater. Chem. A* 5, 12747–12751.
24. Patil, K., Babar, P., Lee, D.M., Karade, V., Jo, E., Korade, S., and Kim, J.H. (2020). Bifunctional catalytic activity of Ni-Co layered double hydroxide for the electro-oxidation of water and methanol. *Sustain. Energy Fuels* 4, 5254–5263.
25. Zhao, J.-W., Li, C.-F., Shi, Z.-X., Guan, J.-L., and Li, G.-R. (2020). Boosting lattice oxygen oxidation of perovskite to efficiently catalyze oxygen evolution reaction by  $\text{FeOOH}$  decoration. *Research 2020*, 1–15.
26. Naderi, A., Yong, X., Karamad, M., Cai, J., Zang, Y., Gates, I., Siahrostami, S., and Wang, G. (2021). Ternary cobalt–iron sulfide as a robust electrocatalyst for water oxidation: a dual effect from surface evolution and metal doping. *Appl. Surf. Sci.* 542, 148681.
27. Zhou, Y., Luo, M., Zhang, Z., Li, W., Shen, X., Xia, W., Zhou, M., and Zeng, X. (2018). Iron-doped cobalt sulfide derived boosted electrocatalyst for water oxidation. *Appl. Surf. Sci.* 448, 9–15.
28. Zhang, J.Y., Lv, L., Tian, Y., Li, Z., Ao, X., Lan, Y., Ji, J., and Wang, C. (2017). Rational design of cobalt–iron selenides for highly efficient electrochemical water oxidation. *ACS Appl. Mater. Interfaces* 9, 33833–33840.
29. Zhang, T., Du, J., Xi, P., and Xu, C. (2017). Hybrids of cobalt/iron phosphides derived from bimetal-organic frameworks as highly efficient electrocatalysts for oxygen evolution reaction. *ACS Appl. Mater. Interfaces* 9, 362–370.
30. Yang, F., Slezberg, K., Sinev, I., Antoni, H., Bähr, A., Ollegott, K., Xia, W., Masa, J., Grüner, W., Cuena, B.R., et al. (2017). Synergistic effect of cobalt and iron in layered double hydroxide catalysts for the oxygen evolution reaction. *ChemSusChem* 10, 156–165.
31. Liu, W., Liu, H., Dang, L., Zhang, H., Wu, X., Yang, B., Li, Z., Zhang, X., Lei, L., and Jin, S. (2017). Amorphous cobalt–iron hydroxide nanosheet electrocatalyst for efficient electrochemical and photo-electrochemical oxygen evolution. *Adv. Funct. Mater.* 27, 1603904.
32. Babar, P., Lokhande, A., Shin, H.H., Pawar, B., Gang, M.G., Pawar, S., and Kim, J.H. (2018). Cobalt iron hydroxide as a precious metal-free bifunctional electrocatalyst for efficient overall water splitting. *Small* 14, 1702568.
33. Li, D., Xing, Y., Yang, R., Wen, T., Jiang, D., Shi, W., and Yuan, S. (2020). Holey cobalt–iron nitride nanosheet arrays as high-performance bifunctional electrocatalysts for overall water splitting. *ACS Appl. Mater. Interfaces* 12, 29253–29263.
34. Jin, H., Mao, S., Zhan, G., Xu, F., Bao, X., and Wang, Y. (2017). Fe incorporated  $\alpha\text{-Co(OH)}_2$  nanosheets with remarkably improved activity towards the oxygen evolution reaction. *J. Mater. Chem. A* 5, 1078–1084.
35. Zhou, P., Wang, Y., Xie, C., Chen, C., Liu, H., Chen, R., Huo, J., and Wang, S. (2017). Acid-etched layered double hydroxides with rich defects for enhancing the oxygen evolution reaction. *Chem. Commun.* 53, 11778–11781.
36. Zhao, J., Wang, X.R., Chen, F.W., He, C., Wang, X.J., Li, Y.P., Liu, R.H., Chen, X.M., Hao, Y.J., Yang, M., et al. (2020). A one-step synthesis of hierarchical porous CoFe-layered double hydroxide nanosheets with optimized composition for enhanced oxygen evolution electrocatalysis. *Inorg. Chem. Front.* 7, 737–745.
37. Cao, L.M., Wang, J.W., Zhong, D.C., and Lu, T.B. (2018). Template-directed synthesis of sulphur doped NiCoFe layered double hydroxide porous nanosheets with enhanced electrocatalytic activity for the oxygen evolution reaction. *J. Mater. Chem. A* 6, 3224–3230.
38. Yue, X., Ke, W., Xie, M., Shen, X., Yan, Z., Ji, Z., Zhu, G., Xu, K., and Zhou, H. (2020). Amorphous CoFe(OH): X hollow hierarchical structure: an efficient and durable electrocatalyst for oxygen evolution reaction. *Catal. Sci. Technol.* 10, 215–221.
39. Han, X., Niu, Y., Yu, C., Liu, Z., Huang, H., Huang, H., Li, S., Guo, W., Tan, X., and Qiu, J. (2020). Ultrafast construction of interfacial sites by wet chemical etching to enhance electrocatalytic oxygen evolution. *Nano Energy* 69, 104367.
40. Yang, Y., Luo, M., Zhang, W., Sun, Y., Chen, X., and Guo, S. (2018). Metal surface and interface energy electrocatalysis: fundamentals, performance engineering, and opportunities. *Chem* 4, 2054–2083.
41. Sanchez, J., Stevens, M.B., Young, A.R., Gallo, A., Zhao, M., Liu, Y., Ramos-Garcés, M.V., Ben-Naim, M., Colón, J.L., Sinclair, R., et al. (2021). Isolating the electrocatalytic activity of a confined NiFe motif within zirconium phosphate. *Adv. Energy Mater.* 11, 2003545.
42. Xiong, Y., Xu, L., Jin, C., and Sun, Q. (2019). Interface-engineered atomically thin  $\text{Ni}_3\text{S}_2/\text{MnO}_2$  heterogeneous nanoarrays for efficient overall water splitting in alkaline media. *Appl. Catal. B Environ.* 254, 329–338.
43. Liu, Y., Jiang, S., Li, S., Zhou, L., Li, Z., Li, J., and Shao, M. (2019). Interface engineering of  $(\text{Ni}, \text{Fe})\text{S}_2@\text{MoS}_2$  heterostructures for synergistic electrochemical water splitting. *Appl. Catal. B Environ.* 247, 107–114.
44. Babar, P., Lokhande, A., Karade, V., Pawar, B., Gang, M.G., Pawar, S., and Kim, J.H. (2019). Bifunctional 2D electrocatalysts of transition metal hydroxide nanosheet arrays for water splitting and urea electrolysis. *ACS Sustain. Chem. Eng.* 7, 10035–10043.
45. Xu, H., Shi, Z.-X., Tong, Y.-X., Li, G.-R., Xu, H., Shi, Z., Tong, Y., and Li, G. (2018). Porous microrod arrays constructed by carbon-confined  $\text{NiCo}@\text{NiCoO}_2$  Core@Shell nanoparticles as efficient electrocatalysts for oxygen evolution. *Adv. Mater.* 30, 1705442.
46. Ledendecker, M., KrickCalderón, S., Papp, C., Steinrück, H.-P., Antonietti, M., and Shalom, M. (2015). The synthesis of nanostructured  $\text{Ni 5 p 4}$  films and their use as a non-NobleBifunctional electrocatalyst for full water splitting. *Angew. Chem. Int. Ed. Engl.* 54, 12361–12365.
47. Rong, M., Zhong, H., Wang, S., Ma, X., and Cao, Z. (2021). La/Ce doped CoFe layered double hydroxides (LDH) highly enhanced oxygen evolution performance of water splitting. *Colloids Surf. A Physicochem. Eng. Asp.* 625, 126896.
48. Cheng, F., Fan, X., Chen, X., Huang, C., Yang, Z., Chen, F., Huang, M., Cao, S., and Zhang, W. (2019). Surface-restructured core/shell

- NiO@Co<sub>3</sub>O<sub>4</sub> nanocomposites as efficient catalysts for the oxygen evolution reaction. *Ind. Eng. Chem. Res.* 58, 16581–16587.
49. Hu, C., Zhang, L., Zhao, Z.J., Luo, J., Shi, J., Huang, Z., and Gong, J. (2017). Edge sites with unsaturated coordination on core-shell Mn<sub>3</sub>O<sub>4</sub>@Mn<sub>x</sub>Co<sub>3-x</sub>O<sub>4</sub> nanostructures for electrocatalytic water oxidation. *Adv. Mater.* 29, 1701820.
50. Zhou, Y., Zhang, W., Hu, J., Li, D., Yin, X., and Gao, Q. (2021). Inherent oxygen vacancies boost surface reconstruction of ultrathin Ni-Fe layered-double-hydroxides toward efficient electrocatalytic oxygen evolution. *ACS Sustain. Chem. Eng.* <https://doi.org/10.1021/acssuschemeng.1c02256>.
51. Babar, P., Lokhande, A., Karade, V., Lee, I.J., Lee, D., Pawar, S., and Kim, J.H. (2019). Trifunctional layered electrodeposited nickel iron hydroxide electrocatalyst with enhanced performance towards the oxidation of water, urea and hydrazine. *J. Colloid Interface Sci.* 557, 10–17.
52. Shi, Z., Yu, Z., Jiang, R., Huang, J., Hou, Y., Chen, J., Zhang, Y., Zhu, H., Wang, B., and Pang, H. (2021). MOF-derived M-OOH with rich oxygen defects by: in situ electro-oxidation reconstitution for a highly efficient oxygen evolution reaction. *J. Mater. Chem. A* 9, 11415–11426.
53. Mo, S., Li, J., Liao, R., Peng, P., Li, J., Wu, J., Fu, M., Liao, L., Shen, T., Xie, Q., et al. (2021). Unraveling the decisive role of surface CeO<sub>2</sub> nanoparticles in the Pt-CeO<sub>2</sub>/MnO<sub>2</sub> heterocatalysts for boosting toluene oxidation: synergistic effect of surface decorated and intrinsic O-vacancies. *Chem. Eng. J.* 418, 129399.
54. Chen, J., Zheng, F., Zhang, S.J., Fisher, A., Zhou, Y., Wang, Z., Li, Y., Xu, B.B., Li, J.T., and Sun, S.G. (2018). Interfacial interaction between FeOOH and Ni-Fe LDH to modulate the local electronic structure for enhanced OER electrocatalysis. *ACS Catal.* 8, 11342–11351.
55. Xie, C., Yan, D., Chen, W., Zou, Y., Chen, R., Zang, S., Wang, Y., Yao, X., and Wang, S. (2019). Insight into the design of defect electrocatalysts: from electronic structure to adsorption energy. *Mater. Today* 31, 47–68.
56. Ananthraj, S., Noda, S., Driess, M., and Menezes, P.W. (2021). The pitfalls of using potentiodynamic polarization curves for Tafel analysis in electrocatalytic water splitting. *ACS Energy Lett.* 6, 1607–1611.
57. Tang, C., Cheng, N., Pu, Z., Xing, W., and Sun, X. (2015). NiSe nanowire film supported on nickel foam: an efficient and stable 3D bifunctional electrode for full water splitting. *Angew. Chem. Int. Ed. Engl.* 127, 9483–9487.
58. Babar, P., Patil, K., Karade, V., Gour, K., Lokhande, A., Pawar, S., and Kim, J.H. (2021). In situ fabrication of nickel–iron oxalate catalysts for electrochemical water oxidation at high current densities. *ACS Appl. Mater. Interfaces* 13, 52620–52628.
59. He, L.G., Cheng, P.Y., Cheng, C.C., Huang, C.L., Hsieh, C.T., and Lu, S.Y. (2021). (Ni<sub>x</sub>FeyCo<sub>6-x-y</sub>)Mo<sub>6</sub>C cuboids as outstanding bifunctional electrocatalysts for overall water splitting. *Appl. Catal. B Environ.* 290, 120049.
60. Babar, P.T., Lokhande, A.C., Shim, H.J., Gang, M.G., Pawar, B.S., Pawar, S.M., and Kim, J.H. (2019). SILAR deposited iron phosphate as a bifunctional electrocatalyst for efficient water splitting. *J. Colloid Interface Sci.* 534, 350–356.
61. Zhao, Y., Gao, Y., Chen, Z., Li, Z., Ma, T., Wu, Z., and Wang, L. (2021). Trifile Pt coupled with NiFe hydroxide synthesized via corrosion engineering to boost the cleavage of water molecule for alkaline water-splitting. *Appl. Catal. B Environ.* 297, 120395.
62. Dinh, K.N., Zheng, P., Dai, Z., Zhang, Y., Dangol, R., Zheng, Y., Li, B., Zong, Y., and Yan, Q. (2018). Ultrathin porous NiFeV ternary layer hydroxide nanosheets as a highly efficient bifunctional electrocatalyst for overall water splitting. *Small* 14, 1703257.
63. Gu, Y., Chen, S., Ren, J., Jia, Y.A., Chen, C., Komarneni, S., Yang, D., and Yao, X. (2018). Electronic structure tuning in Ni<sub>3</sub>FeN/r-GO aerogel toward bifunctional electrocatalyst for overall water splitting. *ACS Nano* 12, 245–253.
64. Zhang, H., Li, X., Hänel, A., Naumann, V., Lin, C., Azimi, S., Schweizer, S.L., Maijenburg, A.W., and Wehrspohn, R.B. (2018). Bifunctional heterostructure assembly of NiFe LDH nanosheets on NiCoP nanowires for highly efficient and stable overall water splitting. *Adv. Funct. Mater.* 28, 1706847.
65. Yan, J., Chen, L., and Liang, X. (2019). Co<sub>9</sub>S<sub>8</sub> nanowires@NiCo LDH nanosheets arrays on nickel foams towards efficient overall water splitting. *Sci. Bull.* 64, 158–165.
66. Dutta, S., Indra, A., Feng, Y., Song, T., and Paik, U. (2017). Self-supported nickel iron layered double hydroxide-nickel selenide electrocatalyst for superior water splitting activity. *ACS Appl. Mater. Interfaces* 9, 33766–33774.
67. Hou, Y., Lohe, M.R., Zhang, J., Liu, S., Zhuang, X., and Feng, X. (2016). Vertically oriented cobalt selenide/NiFe layered-double-hydroxide nanosheets supported on exfoliated graphene foil: an efficient 3D electrode for overall water splitting. *Energy Environ. Sci.* 9, 478–483.